A&A 412, 175–184 (2003)
DOI: 10.1051/0004-6361:20031417

Astronomy & Astrophysics

A massive disk/envelope in shocked H_2 emission around an UCHII region

M. S. N. Kumar[1], A. J. L. Fernandes[1,2], T. R. Hunter[3], C. J. Davis[4], and S. Kurtz[5]

[1] Centro de Astrofísica da Universidade do Porto, Rua das Estrelas, 7150-462 Porto, Portugal
[2] Instituto Superior da Maia, Av. Carlos Oliveira Campos, 4475-690 Avioso S.Pedro, Portugal
[3] Harvard Smithsonian Center for Astrophysics, 60 Garden Street, MS-78 Cambridge, MA 02138, USA
[4] Joint Astronomy Center, 660 N. A'ohōkū Place, University Park, Hilo, HI 96720, USA
[5] Instituto de Astronomia, UNAM-Morelia, Apartado postal 3-72, CP 58090 Morelia, Michoacan, Mexico

Received 23 April 2003 / Accepted 2 September 2003

Abstract. A multi-wavelength study of IRAS 07427–2400 in line and continuum emission was conducted to investigate the nature of a H_2 v = 1–0 S(1) line emitting feature around this ultra-compact HII region. High resolution 3.6 cm continuum observations from the Very Large Array and 350 μm continuum observations from the Caltech Submillimeter Observatory, combined with archival far-infrared data of IRAS 07427–2400 show a flux density distribution indicating a luminous (L = 5.6×10^4 $L_\odot$) point source associated with an ultra-compact HII region. A Grey body model fit to the flux density distribution yields a dust emissivity index ($\beta \sim 0.66$) indicative of a circumstellar disk/envelope. Our $C^{18}O$ map shows a dense core centered on the continuum source, with the major axis roughly aligned with the H_2 feature. A position-velocity diagram of the $C^{18}O$ core obtained along the major axis shows rotation with a velocity gradient of ~0.1 km s^{-1} arcsec^{-1}. New CO J = 3–2 maps of the region are presented which reveal a massive molecular outflow from the IRAS source. We argue that the H_2 feature arises in a disk/envelope around IRAS 07427–2400 and not in an outflow. We present a near-infrared HK band spectrum of the H_2 features that shows several ro-vibrational emission lines of H_2 and [FeII]. Analysis of the line ratios indicates that the line emission is shock-excited and not due to fluorescence. We estimate an excitation temperature of ~1600 K and an average extinction of $A_v \sim 11$ mag to the H_2 feature. The line fluxes yield a mass accretion rate of $\dot{M} \sim 2.6 \pm 0.9 \times 10^{-2}$ $M_\odot$ yr^{-1} and a lifetime of ~5360 ± 1200 yr resulting in a disk/envelope mass of 140 ± 50 $M_\odot$. The resulting Jeans Mass of 2420 $M_\odot$ indicates that the disk/envelope will not undergo fragmentation. IRAS 07427–2400 represents one of the most massive YSOs known to date forming by means of accretion.

Key words. stars: formation – accretion: accretion disks – interstellar medium: jets and outflows – ISM: HII regions

1. Introduction

Circumstellar disks are known to exist around low mass young stellar objects (YSOs) (see Beckwith 1999; Beckwith & Sargent 1996). Disks around low mass stars have mostly been detected by imaging the continuum emission from warm dust (Dutrey et al. 1996) or in the visible as extincted patches seen in silhouette against background light (Padgett et al. 1999; Bally et al. 2000). Observational studies of circumstellar disks around YSOs provide important evidence supporting the accretion-driven mechanism of star formation (see Shu et al. 2000). If stars of all masses form in the same way, through an accretion mechanism, disks should exist around massive YSOs and brown dwarfs in much the same way they do around low mass YSOs. Recently, the existence of disks around brown dwarfs has been demonstrated using indirect methods such as color–color diagrams (Muench et al. 2001). In a few cases of massive protostars, disks have been shown to exist through observations of molecular lines (Cesaroni et al. 1999; Shepherd et al. 2001; Zhang et al. 2001).

A class of objects known as Infrared Companions (IRC) to T Tauri stars are found to show a near-infrared excess due to ongoing accretion (see Herbst et al. 1995; Koresko et al. 1997). In particular, IRCs to T Tauri, UY Aurigae and Haro 6-10 were found to emit intense H_2 emission which is attributed to energetic phenomena associated with accretion shocks and magnetic fields (Koresko et al. 1997). Recently, Kumar et al. (2002, hereafter KBD02) showed the presence of rings and disk-like structures visible in H_2 emission around massive YSOs. These structures may also be explained by accretion shocks and magnetic fields, especially when one considers the much higher density of material and gravitational potential around a massive star. To further investigate this possibility we present here a systematic study of IRAS 07427–2400.

Send offprint requests to: M. S. N. Kumar,
e-mail: nanda@astro.up.pt

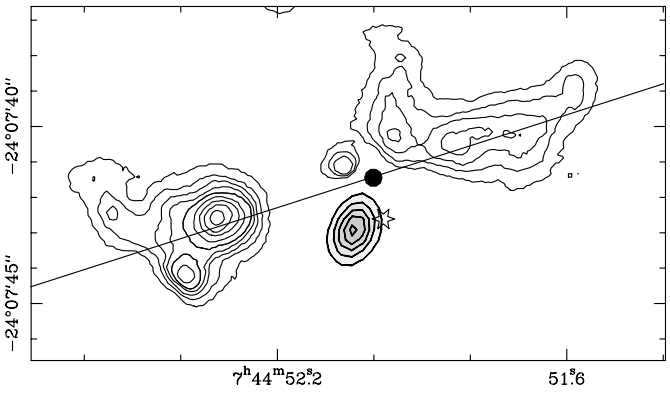

Fig. 1. Continuum subtracted H_2 2.121 μm emission contours around IRAS 07427–2400 with levels 5, 7, 9, 11, 15, 19, 23, 27 and 31σ above the mean background. The filled circle marks the position of a 2 μm star that is subtracted from the line+continuum narrow-band image. Thick contours and shades of grey show VLA 3.6 cm continuum emission at levels of 2, 4, 6, 8, 10 mJy. The star symbol represents the position of the IRAS Point Source.

2. Observational data

We present near-infrared spectroscopic observations obtained with the UIST instrument at UKIRT in December 2002. The 4 pixels wide, 120 pixels long slit was positioned along the main H_2 emission features at a Position Angle (PA) = 107.5° as shown in Fig. 1. The spectra were obtained with a plate scale of 0.12″/pixel, with simultaneous H and K-band coverage. The observed lines are unresolved with a spectral resolution $R \sim 630$ or $\Delta v \sim 480$ km s^{-1}. Standard data reduction techniques were employed including dark-subtraction and flat-field division. Wavelength calibration was done with argon arc spectra and flux calibration and correction for atmospheric absorption via division by a standard star spectrum.

3.6-cm continuum emission maps were obtained using the Very Large Array (VLA) in its B configuration. The beam size was 1.8″ × 0.8″ and the observations were sensitive to structures up to 15″. 350 μm continuum emission and CO J = 3–2 and $C^{18}O$ J = 2–1 line emission were mapped using the Caltech Submillimeter Observatory 10.4 m telescope at Mauna Kea, Hawaii. 350 μm emission was mapped using the SHARC bolometer array with a pixel size of 5″. The secondary chopper throw was 86″ in azimuth at 4.1 Hz. Calibration was based on scans of Uranus with an airmass correction (the measured opacity in the filter band was 0.63). Images were restored and smoothed to a 12″ beam. CO J = 3–2 maps were obtained with a grid size of 10″ and $C^{18}O$ J = 2–1 maps with a grid size of 15″. The standard facility SIS Heterodyne receivers and acousto-optical spectrometers were utilized.

3. IRAS 07427–2400 and the nature of the H_2 features

3.1. UCHII region, continuum sources and the dense core

IRAS 07427–2400 is a far-infrared (FIR) point source (d = 6.4 kpc) with a luminosity of $L = 5 \times 10^4$ $L_\odot$ suggesting an O8.5 spectral type zero-age main-sequence (ZAMS) star (Panagia 1973). It is known to be associated with OH masers (MacLeod 1991; Smits 1994; Slysh et al. 1997) and H_2O masers (Henning et al. 1992). KBD02 discovered a disk-like structure in H_2 emission around this FIR source. In Fig. 1 we show continuum subtracted H_2 v = 1–0 S (1) 2.122 μm emission features (thin contours) around IRAS 07427–2400. Thick-lines along with greyshades are used to overlay the VLA 3.6 cm continuum emission in the same region. The star symbol shows the center of the IRAS error ellipse and the filled circle shows the position of a 2 μm continuum source visible in the H_2 narrow-band image. The straight line at PA 107.5° marks the position of the slit used to obtain the near-infrared HK spectrum shown in Fig. 7. This line also indicates the axis of the bipolar H_2 feature. The astrometry of the VLA data and the H_2 image are accurate to better than 1.5″ and are the most precise among all the available data on this source. These images also represent the highest spatial resolution data available for this target. The radio source is unresolved by the VLA beam, indicating a source size smaller than 0.3″ × 0.2″. This is in good agreement with the 6 cm data of Hughes & MacLeod (1993) who report the source as unresolved at 0.3″ resolution. It can be seen from Fig. 1 that the VLA continuum source, FIR source and the 2 μm source are all situated centrally (within positional uncertainties of <1.5″) to the bipolar H_2 emission feature. Accounting for astrometric errors, the unresolved VLA source, the IRAS point source and the 2 μm star all represent the same object, namely IRAS 07427–2400.

A summary of the flux density measurements for this region (along with the corresponding beamsizes) is given in Table 1. These values (except for the FIRSSE values) are plotted in Fig. 2, along with a family of greybody models. The infrared through sub-millimeter flux densities cannot be fit by a single temperature greybody spectrum. In lieu of a radiative transfer model, we have chosen to fit only the cold component of the emission (60−350 microns), as it contains the bulk of the source luminosity. Since the chopper throw of the 350 μm observations is larger than the fitted size of the IRAS 60 μm data (both the HIRES beam and source image), we have assigned all of the 60 and 100 μm emission to the 350 μm source. A complete grid of models was calculated with the parameters being temperature (T), dust emissivity index (β) and optical depth ($\tau_{125\ \mu m}$). The best-fit model has T = 46 K, β = 0.66 and $\tau_{125\ \mu m}$ = 0.05. To estimate the uncertainty of the results, we also fit models to each combination of the 1-sigma uncertainties in the three measured flux densities. The full range of fitted values and the derived physical quantities are listed in Table 2. The value for β is not well-constrained, mainly due to the lack of a millimeter wave flux measurement. The models range from 2−14 Jy in their prediction at 1.3 mm, thus a future measurement there would be useful. Nevertheless, β appears to be significantly less than the typical value of 2 seen in interstellar gas (Hildebrand 1983) and is more consistent with grain growth (or high optical depth) as seen toward the central peak of low-mass protostellar objects (e.g. Hogerheijde & Sandell 2000). In any case, the range of values for the luminosity and mass of the dust emission are consistent with the presence of a deeply embedded massive young stellar object.

Table 1. Infrared flux densities of IRAS 07427–2400.

Wavelength (μm)	Flux density (Jy)	Fitted size	Beamsize	Telescope
8.3	0.635 ± 0.032	52″ × 31″	~24″	MSX/SPIRITIII
12	1.96 ± 0.08	–	–	IRAS/PSC
12.1	2.20 ± 0.07	33″ × 23″	~25″	MSX/SPIRITIII
14.7	3.67 ± 0.15	25″ × 21″	~25″	MSX/SPIRITIII
20[a]	20	–	2.5′ × 10′	FIRSSE
21.3	31.2 ± 1.9	27″ × 22″	~26″	MSX/SPIRITIII
25	64 ± 2	46″ × 25″	48″ × 23″	IRAS/HIRES
27[a]	69	–	2.5′ × 10′	FIRSSE
40[a]	142	–	4.0′ × 12′	FIRSSE
60	613 ± 25	67″ × 47″	68″ × 39″	IRAS/HIRES
100	780 ± 55	91″ × 87″	96″ × 75″	IRAS/HIRES
352	119 ± 36	20″ × 19″	12″	CSO/SHARC

[a] Data from Gezari et al. (1993); Seal & Shivanandan (1989) (FIRSSE #223).

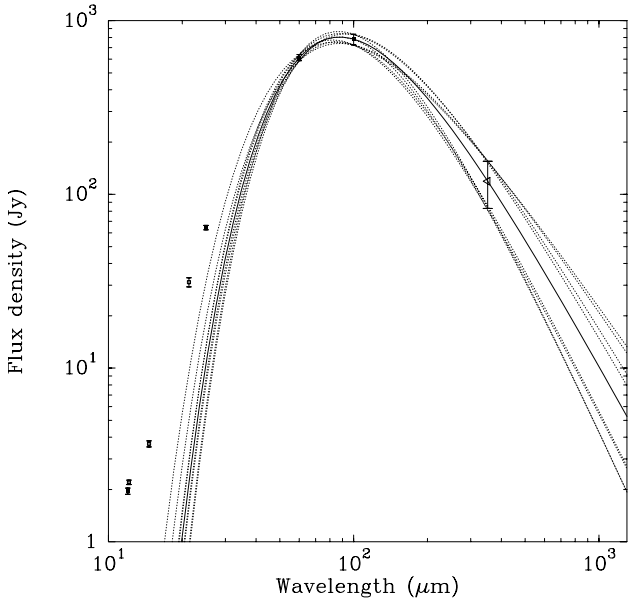

Fig. 2. Flux density distribution of IRAS 07427–2400 with a family of one-component greybody models. As listed in Table 1, solid squares are from IRAS, open squares are from MSX and the triangle is from SHARC (this paper). The solid line marks the best fit to the 60, 100 and 350 micron flux densities (with zero degrees of freedom). The eight dashed lines describe models which pass through the 1-sigma uncertainties of the flux densities. The corresponding range of fitted values and derived physical properties are listed in Table 2. The curve that comes closest to the mid-infrared data is the one most like a blackbody (i.e. $\beta = 0.09$).

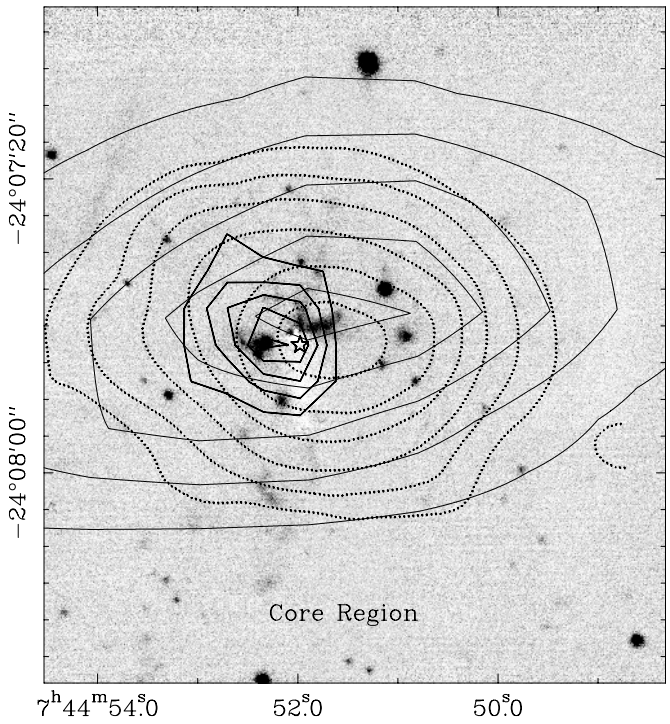

Fig. 3. HIRES processed IRAS 12 μm emission (thin contours) overlaid on the H_2 grey scale image. Thick contours represent 350 μm emission with levels from 30 Jy/beam to 110 Jy/beam increasing in steps of 20 Jy/beam. Dashed contours show integrated $C^{18}O$ emission with levels plotted from 2 K km s^{-1} to 7 K km s^{-1} increasing in steps of 1 K km s^{-1}. The star symbol represents the position of IRAS 07427–2400.

In Fig. 3 we show the 350 μm continuum emission, $C^{18}O$ emission map and HIRES processed IRAS 12 μm map overlaid on the H_2 image. These tracers arise from the dense core of a star forming region. The 350 μm emission that largely traces the cold dust in dense cores is found to be uniformly distributed on IRAS 07427–2400 and also encloses the H_2 emission feature. The $C^{18}O$ emission is concentrated in a central ellipse of 20″ × 33″ (0.64 pc × 1.07 pc). The major axis of the $C^{18}O$ core is roughly aligned with that of the H_2 feature. A position–velocity (*PV*) diagram along this axis is shown in Fig. 4. It can be seen that the eastern and western edges of the $C^{18}O$ core are doppler shifted to red and blue respectively from V_{lsr} = 67.5 km s^{-1}, implying a rotating core. Further,

Table 2. Derived physical properties of IRAS 07427–2400.

Physical parameter	Best fit value	Uncertainty range
T (K)	46	41–59
β	0.66	0.09–1.20
$\tau_{125\mu m}$	0.050	0.026–0.075
log ($\bar{N}_H$)	23.07	22.78–23.13
log ($L/L_\odot$)	4.75	4.71–4.79
log ($M/M_\odot$)	2.59	2.30–2.76
L/M	144	95–310
log ($\bar{n}_H$)	4.78	4.49–4.96

The above calculations assume a distance of 6.4 kpc.

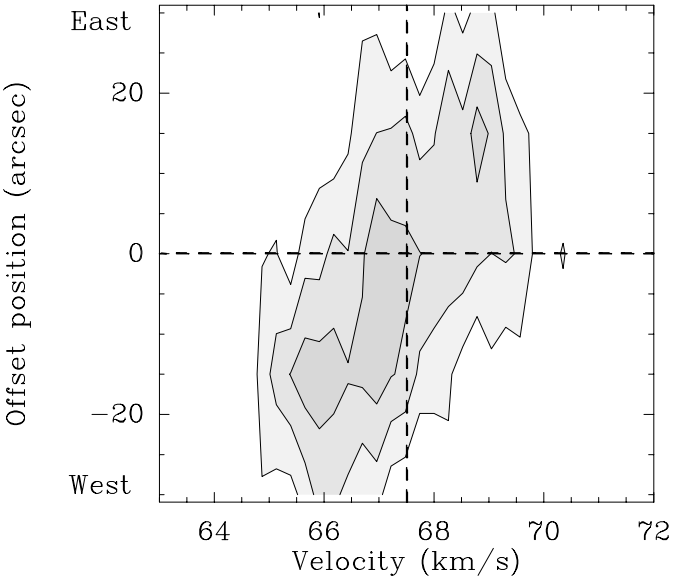

Fig. 4. Position–velocity diagram of the $C^{18}O$ core along the major axis aligned East-West. The emission is summed over a width of 45″ in the north-south direction representing the minor axis of the core (see Fig. 3). Contours begin at 0.6 K km s^{-1} and increase in steps of 0.3 K km s^{-1}.

it can be seen that the velocity spread at the center of the core is larger (∼5 km s^{-1}) compared to that at the edges (∼2 km s^{-1}), implying that the center of the core is rotating much faster than the edges. A straight line fit to the *PV* diagram results in a velocity gradient of ∼0.1 km s^{-1} arcsec^{-1} and indicates approximately Keplerian rotation. The area averaged $C^{18}O$ line widths are ∼3.4 km s^{-1}. Note that these velocities are similar to the line widths of $H^{13}CO^+$ profiles (∼3 km s^{-1}) measured by Cesaroni et al. (1999) in the case of a disk around IRAS 20126+4104, a prototypical massive protostar. *The continuum emission and the $C^{18}O$ data together show that the H_2 feature arises in the plane of a rotating disk/envelope surrounding IRAS 07427–2400.*

3.2. Bipolar outflows from IRAS 07427–2400

Figures 5 and 6 show the bipolar molecular outflows around IRAS 07427–2400. In Fig. 5 we reproduce the CO J = 1–0 contour map from Shepherd & Churchwell (1996, hereafter SC96) overlaid on the H_2 grey scale image from KBD02. The CO J = 1−0 outflow is well-centered on IRAS 07427–2400, shown by a star symbol. The PA of the outflow axis is between 20° and 30° as measured from Fig. 6 of SC96. These authors argue that the CO J = 1–0 emission traces a massive molecular outflow from IRAS 07427–2400. They estimate an outflow mass of 8.3 $M_\odot$, a momentum of 93 $M_\odot$ km s^{-1}, and a timescale of 2.3×10^4 yr, resulting in a mechanical luminosity of ∼3.9 $L_\odot$. This is an order of magnitude higher than that of L1551 IRS5, a prototypical outflow from a low mass protostar (Fridlund et al. 1989).

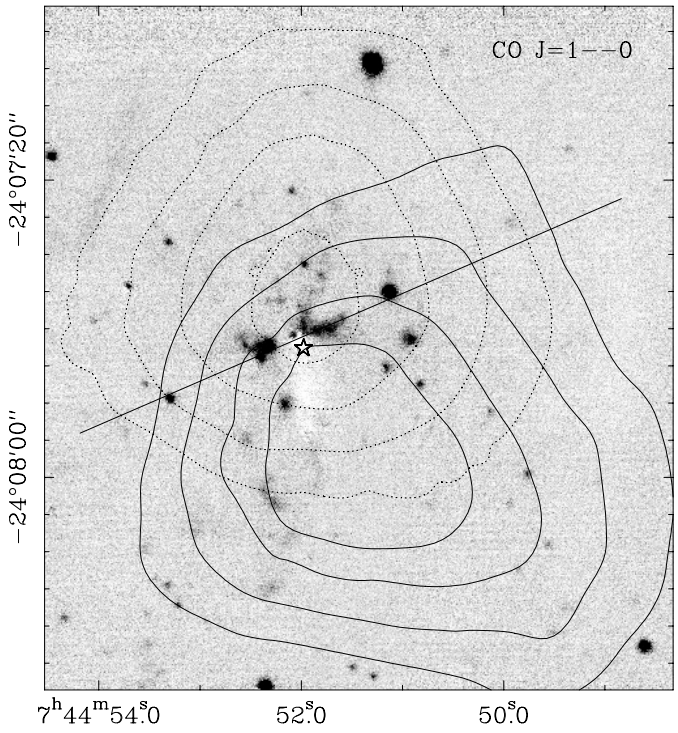

Fig. 5. CO J = 1–0 high velocity emission contours from SC96 overlaid on a continuum subtracted H_2 image at 2.122 μm. Red-shifted (dotted lines) contours are 0.5, 0.75, 1, 1.2 K km s^{-1} and blue-shifted (solid lines) contours are 0.3, 0.45, 0.6 and 0.7 K km s^{-1}. The star symbol represents the position of the IRAS Point Source.

In Fig. 6 we present new maps of CO J = 3–2 integrated high velocity emission overlayed on to the grey scale H_2 image. Figures 6a and 6b show channel maps that separate low and high velocity components. The velocity shifts are with respect to V_{lsr} = 69 km s^{-1}. The CO J = 3–2 emission shows a prominent bipolar outflow at PA ∼ 132° and a weaker component at PA ∼ 101°. The weaker component is at relatively lower velocities of ±6−11 km s^{-1} while the main flow has velocity components extending up to ±17 km s^{-1}. We estimate a total mass of 36 $M_\odot$, momentum of 253 $M_\odot$ km s^{-1} and an outflow timescale of 1.5×10^5 yr, resulting in a CO mechanical luminosity of ∼1 $L_\odot$.

It appears from Figs. 5 and 6 that there are at least two massive outflows in the region at different position angles. The first question that arises is whether the flows traced by CO J = 1−0 and CO J = 3−2 are really different. The half

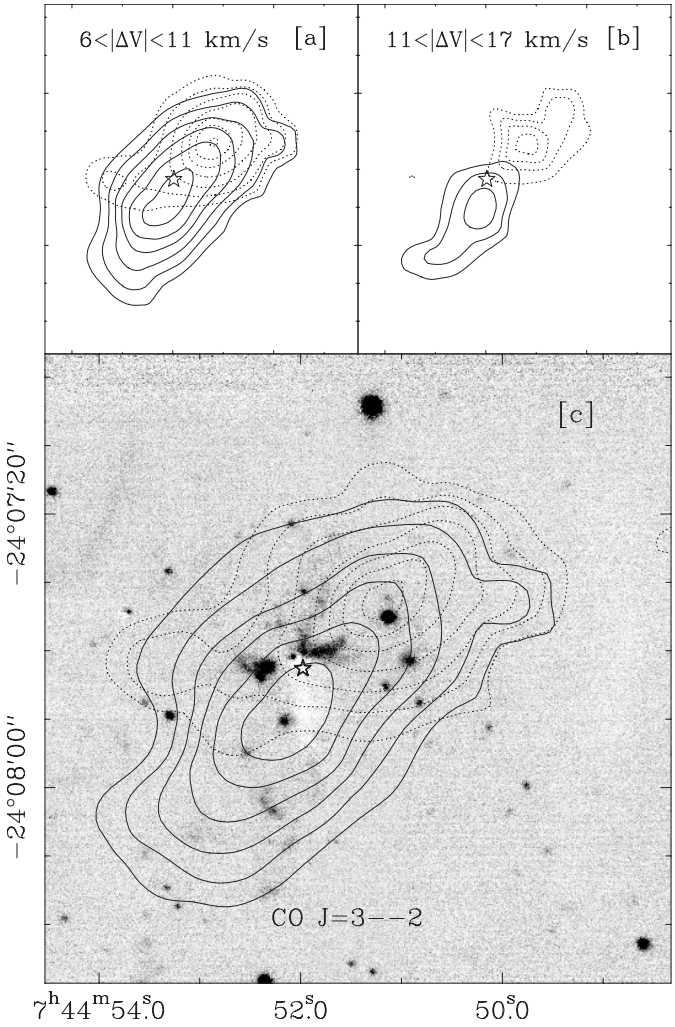

Fig. 6. CO J = 3–2 high velocity emission contours overlayed on a continuum subtracted H_2 grey scale image. **a)**, **b)** Channel maps in velocity intervals (w.r.t $v_{\rm lsr}$ = 69 km s^{-1}) printed within the respective boxes. **c)** Red-shifted (dotted lines) and blue-shifted (solid lines) emission are integrated from ±6 to ±17 km s^{-1}. Red-shifted contour levels start at 4 K km s^{-1} and blue-shifted contours starts at 10 K km s^{-1} and both increase in steps of 6 K km s^{-1}. The star symbol represents the position of the IRAS Point Source.

power beam width of the CO J = 1–0 map is 60″ while that of the CO J = 3–2 map is 20″. Given the large difference in resolution and the possibility that gas in different parts of the outflow lobes are at different temperatures, these maps may trace the same outflow. However, the axes of the flows differ in PA by ∼60° over an extent of 90″, which cannot be easily explained by differing angular resolution. This effect could be produced if the CO J = 1–0 traces a larger angular extent than CO J = 3–2. Mapping the outflow in both lines with similar angular resolution can resolve this issue. In any case, the axes of these two outflows do not coincide well with the axis of the H_2 feature. The mean PA (∼25°) of the CO J = 1–0 outflow is nearly perpendicular to the axis of the H_2 emitting feature (PA ∼ 108°). The PA of the high velocity CO J = 3–2 outflow is also clearly about 30° away from the H_2 axis. Only the low velocity component at PA ∼ 101° is spatially well-correlated with the axis of the H_2 feature.

It is well-known that H_2 emission and CO outflows are spatially well-correlated (see Davis & Eislöeffel 1995; Bachiller 1996) where H_2 traces the cavities of the CO outflow. The fainter H_2 features along the North-South direction that appear as nested bows (see KBD02) could delineate the cavity boundaries of the CO J = 1–0 emission along the red and blue lobes. Further, H_2 emission associated with outflows is known to appear as jets/knots that generally show increasing collimation with increasing distance from the driving source. The dominant H_2 feature resembles the morphology of a disk more than that of a jet/outflow. Also the H_2 emission is bright only near the source and abruptly terminates beyond 5″ – a behavior that is extremely unlikely to be observed in outflows. *Therefore, the H_2 feature shown in Fig. 1 is probably not a part of the massive CO outflow, but rather arises in a disk-like structure associated with the low velocity component of the CO J = 3–2 emission.*

The presence of CO outflows, $C^{18}O$ and dust emission at 350 μm all coinciding with the H_2 feature indicates the existence of dense, cold, neutral material around the H_2 feature. Therefore, the physical condition producing the H_2 emission is also expected to show its signatures in the molecular lines of CO which is more easily excited than H_2. However, such a detection strongly depends on the beam filling factor of the feature and the signal-to-noise ratio. The H_2 emitting region is much smaller than the CO emitting region so the beam filling factor is expected to be very low, resulting in difficulties to identify the feature in CO lines. The feature will probably show up well in high J sub-millimeter CO lines (e.g., 7–6) that have upper level energies >150 K, and perhaps even lower J lines with the use of interferometers.

4. H_2 line emission analysis

In this section we present the analysis of a near-infrared H & K band spectrum obtained on the putative disk-like H_2 feature, in order to evaluate the H_2 excitation mechanism. The near-infrared H & K band spectrum was obtained with the slit placed along the equatorial axis of the possible star-disk system as shown in Fig. 1. Two spatial cuts along the slit were extracted to identify the emission from STAR and DISK. The continuum strip on the spectral images that fell on the middle 10 pixels enclosing the 2 μm visible star (width of 1.2″) was extracted as the STAR spectrum which likely includes contributions from the unresolved UCHII region. The remaining parts of the spectrum that were visible only in emission lines and associated with the extended H_2 feature were summed (over 70 pixels) to obtain the DISK spectrum. In Fig. 7 we present these two spectra separately with the STAR spectrum displayed in the top panel and the DISK spectrum displayed in the bottom panel. The most prominent features in the K band are the H_2 emission lines arising from several ro-vibrational transitions. In the H band we have detected the $a^4D_{7/2}$–$a^4F_{9/2}$ 1.644 μm and the $a^4D_{7/2}$–$a^4F_{7/2}$ 1.810 μm [FeII] lines and the v = 1–0 S (6) and S (7) H_2 emission lines. Unlike the DISK spectrum, the STAR spectrum includes strong detections of Brackett 10 in the H band plus Br γ in the K band. Comparing the K window spectra at

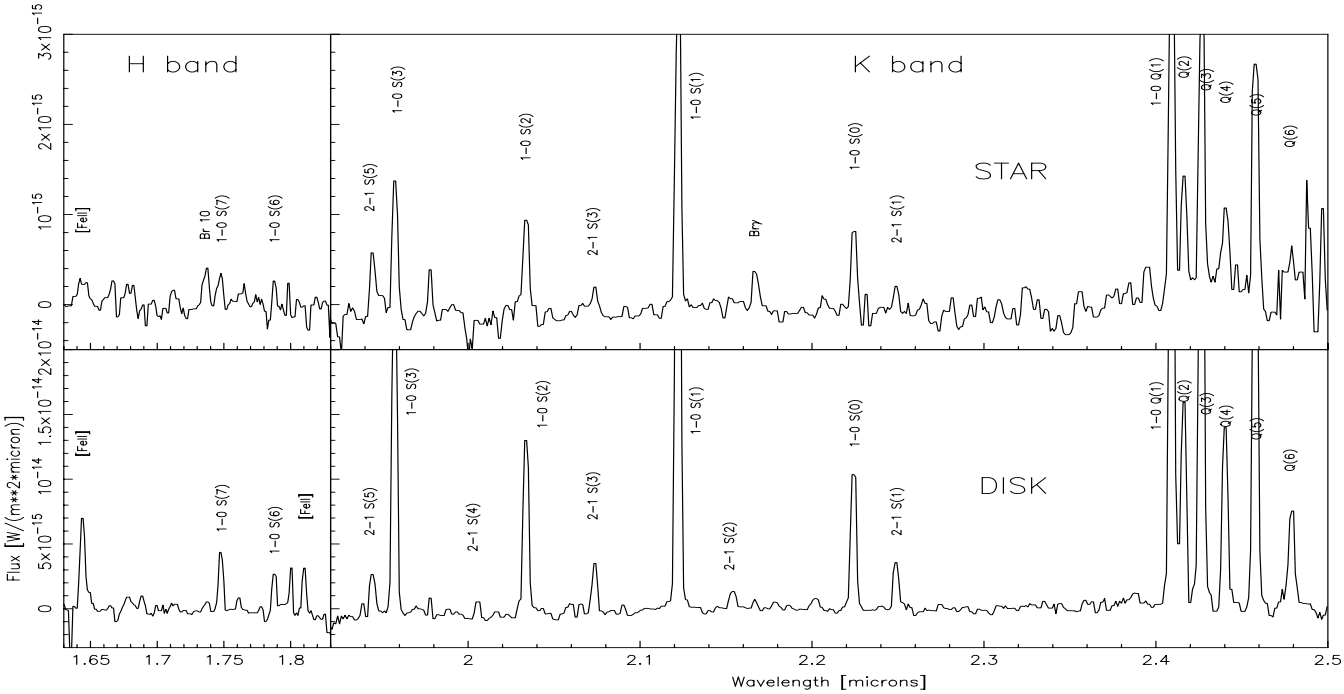

Fig. 7. Near-infrared H and K–band spectra of the H_2 emitting feature shown in Fig. 1. The top panel displays the spectrum of the middle 1.2″ region centered on the 2 μm star marked by a filled circle in Fig. 1. The bottom panel shows the spectrum of the remaining disk-like feature displayed in thin contours in Fig. 1.

both positions, we noticed an unusually bright v = 2–1 S (5) H_2 line appearing in the STAR spectrum when compared to the other v = 2–1 line fluxes. For example, the 2−1 S (5)/S (1) line ratio for the DISK spectrum is $\sim 0.8 \pm 0.2$ whereas for the STAR this ratio is $\sim 2.8 \pm 0.8$. This apparent enhanced emission from the high vib-rotational v = 2, J = 8 H_2 level may arise due to more energetic conditions close to the star. However, the atmospheric transmission near the 1.95 μm lower end of the K window makes the line fluxes very uncertain. For this reason, in the following analysis we do not use the 2−1 S (5) and the 1−0 S (3) lines, but rely upon the remaining lines. Thus, we computed line fluxes for all the remaining H_2 lines detected in the spectra by fitting single or multiple Gaussian profiles to account for line blending.

4.1. The reddening

The amount of reddening due to foreground extinction can be estimated by using a pair of H_2 emission lines arising from a common upper level. The intensity ratio of such lines is uniquely determined by known physical parameters and the extinction value and does not depend on the excitation mechanism (see e.g., Fernandes et al. 1997). The near-infrared K-band contains several rotational transitions of the H_2 v = 1 to v = 0 emission line pairs such as [S (1), Q (3)] and [S (0), Q (2)]. In practice, only the strongest observed line pair is used since the Q-lines are present at the edge of the K-band atmospheric window, which precludes an accurate determination of the absolute line fluxes. Therefore, we have used the [S (1), Q (3)] line pair to estimate the differential extinction from 2.121 to 2.406 μm. The extinction at any other wavelength can then be determined by adopting the extinction law: $A_\lambda \propto \lambda^{-1.7}$ valid for the near-IR wavelengths (Draine 1989). The visual extinction can then be determined by assuming $A_v = 10 \times A_K$. The estimated visual extinction found for the (STAR+DISK) emission is 11.2 ± 1.6 mag. We found that the inner STAR region (A_v = 16.1 ± 2.8) is more extincted than the outer DISK region (A_v = 10.7 ± 1.5) by $A_v \sim$ 5.4 mag. The dust emission model column density range (see Table 2) predicts 15−33 mag of A_v assuming that the source is placed at the center of the cloud (and using a conversion factor of 2×10^{21} cm^{-2} per mag). This range actually contains the A_v predicted above from the near-infrared spectrum.

4.2. H_2 column densities and excitation temperatures

Conversion of all the intrinsic fluxes to column densities of the upper transition levels provides a tool to inspect the H_2 population and thus infer the gas excitation conditions. Figure 8 shows the derived column density diagram of the observed H_2 lines for the total (STAR+DISK) emission. If the shocked gas is relaxed at some temperature then the H_2 levels will be populated according to a Boltzmann distribution and in Fig. 8 the data points should fall in a straight line where the slope is inversely proportional to the excitation temperature of the gas. In Fig. 8 we show the v = 1 upper level data points by squares and v = 2 upper level data points by triangles along with their corresponding error bars. A linear fit to the data indicates an excitation temperature of 1600 ± 200 K for the H_2 emission feature. Filled circles in Fig. 8 show the predicted positions for fluorescent excited H_2 population according to the models of Black & van Dishoeck (1987). Shock and fluorescent

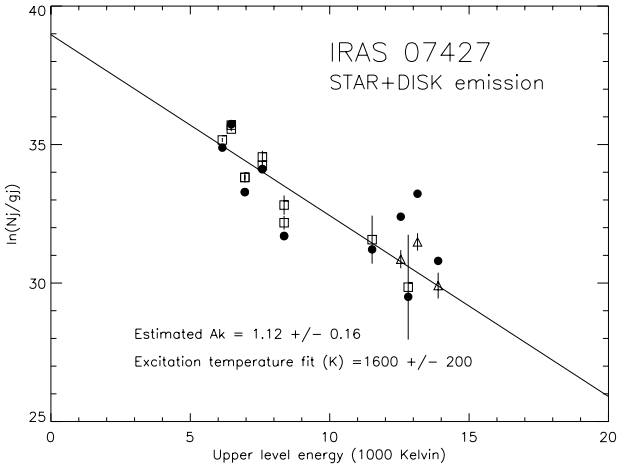

Fig. 8. Diagnostic diagram showing the dereddened H_2 column densities versus the upper level energy in Kelvin. The diagram plots the natural logarithm of the column density divided by the statistical weight, against the upper energy level for each line transition. The plotted lines arise from vibrational levels $v = 1$ (squares) and $v = 2$ (triangles). The straight line represents the best linear fit through the observed data points. Filled circles are predictions from Black & van Dishoeck (1987) for fluorescent excitation.

excitation can be discerned clearly only by observations of emission lines with upper energy levels of $v = 2$ or higher. Our data shows only emission lines originating from $v = 1$ and $v = 2$ upper levels. Nevertheless, the model predictions of fluorescent excitation (for $v = 2$ levels) clearly lie above the observed points (shown by triangles) indicating that the observations do not support fluorescent excitation. Thus the observed H_2 emission is understood to be originating from shock waves. Separate diagrams made for each region show remarkable similarity of the H_2 excitation temperature along the observed emission axis. Within the errors, the excitation temperature derived for the DISK region of 1544 ± 230 K is similar to the value obtained for the STAR region of 1338 ± 188 K. The presence of strong [FeII] lines is expected in fast discontinuous shocks (J-shocks) where shock velocities exceed 50 km s^{-1} (Hollenbach & McKee 1989). J-shocks would completely dissociate H_2, however, so either H_2 reforms in a region downstream from the supersonic shock front or the H_2 is excited in weaker continuous shocks (C-shocks) that are softened by magnetic fields closer to the central source.

4.3. Br γ emission

The STAR spectrum displayed in the top panel of Fig. 7 shows Br γ emission. This emission is an average measured within 1.2″ of the 2 μm star. Since the seeing was less than 1.2″ we expect that the STAR essentially encloses all the contribution from the massive young star and the UCHII region which is shown to be smaller than 0.3″ (see Sect. 3.1). Using line fits to the spectrum, we measured a flux of $2.71 \pm 0.67 \times 10^{-22}$ W cm^{-2} arcsec^{-2}. After correcting for the extinction in the central region ($A_k = 1.61 \pm 0.28$ mag), we obtain a Br γ flux of $1.2 \pm 0.3 \times 10^{-21}$ W cm^{-2} arcsec^{-2}. The Br γ flux predicted for a 100 km s^{-1} J-shock with a number density of 10^5 cm^{-3} is about 1×10^{-21} W cm^{-2} arcsec^{-2} (see Burton et al. 1989). This is in close agreement with the measured flux for the STAR spectrum implying that the observed Br γ flux can arise in fast J-shocks anywhere within the inner 6000 AU envelope to the star; although contributions from an UCHII region cannot be ruled out. In comparison, a much higher level of Br γ flux is observed in the DR21 outflow where fluorescent excited H_2 emission is detected (Fernandes et al. 1997). The presence of [FeII] emission in the DISK spectrum indicating shocks up to 50 km s^{-1} in the outer envelope and Br γ in the STAR spectrum indicating shocks up to 100 km s^{-1} in the inner envelope thus strongly support that the envelope as a whole is dominated by shocks rather than fluorescence.

5. Discussion

5.1. Continuum and molecular line data

The central placement of the continuum sources and the UCHII region over the bipolar H_2 feature of Fig. 1 shows that the FIR source IRAS 07427–2400 is the center of this emission. The uniform distribution of the $C^{18}O$ and 350 μm emission over the IRAS source and the H_2 feature indicates a dense core that encloses them. The grain emissivity index β set as a free parameter in our grey-body model fits indicates a value $\beta \sim 0.66$ which is much less than the value found in the average interstellar medium where $\beta \sim 2$. Indeed, it is similar to that of a circumstellar disk such as HL Tau ($\beta = 0.9$, see Beckwith & Sargent 1991). It is now fairly well established that circumstellar disks have $\beta \leq 1$ due to the growth of particle sizes (Beckwith et al. 2000). This is true even for large circumstellar envelopes of few thousand AU radii (Hogerheijde & Sandell 2000). Therefore the observed value of β in IRAS 07427–2400 indicates the presence of a circumstellar disk/envelope structure whose dimensions are larger than the H_2 emission feature.

As shown in Sect. 3.2 the H_2 feature arises *not* in the plane of the outflow axis but in a nearly perpendicular plane. The fainter component of CO $J = 3$–2 at low velocities of ± 6–11 km s^{-1} at PA $\sim 101°$ matches closely with the axis of the H_2 feature. Thus we infer that most of the slow moving gas in the envelope is restricted to this plane which is also the major axis of the $C^{18}O$ core. Since the $C^{18}O$ core shows evidence for Keplerian rotation, we can compute the net mass enclosed within the radius of the observed core. For a spherical envelope of gravitating mass in virial equilibrium, $v^2 = GM/R$, where M is the mass of the material moving with velocity v inside a radius R. The velocity gradient of 0.1 km s^{-1} arcsec^{-1} derived from the PV diagram and the projected radius $R = 0.62$ pc of the $C^{18}O$ core implies a velocity $v = 2$ km s^{-1} and an enclosed mass of $M = 625\ M_\odot$. Note that the single component grey-body fit (Fig. 2) predicts a source mass of ~400 $M_\odot$ (see Table 2). While the source can account for two-thirds of the above mass, the remaining one-third of ~200 $M_\odot$ can be attributed to the mass of a surrounding torus. These pieces of evidence suggest that the H_2 emitting feature arises from a huge rotating torus in the disk plane. Such tori/envelopes are known to exist in other massive YSOs (Shepherd & Kurtz 1999; Cesaroni et al. 1999).

5.2. Implications of HK spectral analysis

As shown in Sect. 4.2 the line ratios indicate the purely shocked nature of the H_2 emission. Emission lines that can be attributed to the presence of intense ultra-violet light are found only within the central 1.2″ enclosing the STAR and the UCHII region. Both Br γ and Brackett 10 are bright only in the STAR spectrum. The compact nature of the HII region ($\sim 0.3'' \times 0.2''$) indicates that the ionizing radiation from the central source influences only the inner 1000 AU radius and is unable to affect the larger ~33 000 AU structure. The H_2 gas is found to be in equilibrium at a temperature of ~1600 K.

There is still much controversy about the nature of shocks occurring in molecular cloud cores. C-type shocks, strongly dependent on a significant ambient magnetic field entrained in a low ionization gas cloud, have been modeled to produce significant column densities of warm H_2 gas at gas temperatures below 16 000 K for $n_H \sim 10^3$ cm^{-3} or below 4000 K for $n_H \sim 10^8$ cm^{-3} (Le Bourlot et al. 2002). On the other hand, J-type shocks form in relatively high degree of ionization gas regions, where magnetic fields are too weak generating a single fluid hydrodynamic shock wave (e.g., Smith 1994). H_2 can be excited in J-shocks with velocities as low as 8–10 km s^{-1} and can be observed in reformation zones when velocities reach up to 200 km s^{-1}.

But the excitation of [FeII] requires J shocks with velocities of at least 40–60 km s^{-1} for pre-shock gas densities of 10^4 cm^{-3}. The presence of both H_2 and [FeII] lines in the spectrum strongly suggests the presence of J type shocks rather than C shocks since [FeII] cannot be excited in the presence of C shocks alone (Gredel 1994). The unreddened H_2 1−0 S(1) line intensity of 1.3×10^{-16} W m^{-2} arcsec^{-2} is about 3 times larger than the [FeII] 1.644 μm line intensity of 4.4×10^{-17} W m^{-2} arcsec^{-2}. Such a high value can only be modelled with fast J-shocks of 80−100 km s^{-1} in gas density of 10^4 cm^{-3} (Hollenbach & McKee 1989; Smith 1994). Moreover, we computed the unreddened column density of the $v = 1$, $J = 3$ upper level (from where the 1−0 S(1) H_2 line arises) to be 1.0×10^{16} cm^{-2}, a value that is well-explained by slow, non-dissociative J-shock models (Smith 1994). This result can be compared with HH120, where Nisini et al. (2002) found the H_2 1−0 S(1)/[FeII] 1.644 μm ratio to be 4.5 which they modeled with fast J shocks. On the other hand, C-type shocks with velocities above 20 km s^{-1} produce much larger columns of warm gas in the $v = 1$, $J = 3$ excited level of ~10^{17}–10^{19} cm^{-2} (Smith 1993) which are not observed here. *It thus appears that C-shocks cannot explain the observed H_2 emission.*

The observed H_2 spectrum also suggests that most of the gas is shocked by low velocity non-dissociative shocks. If dissociative shocks *alone* were present, H_2 would dissociate and reform behind the shock front. H_2 recombines through higher vibrational levels of $v = 6$ (Black & van Dishoeck 1987) resulting in brighter lines from levels of $v > 3$. This is not seen in our spectrum (see Fig. 7) indicating the absence of higher velocity J shocks. Moreover, H_2 reforms in gas at much lower temperatures than the value obtained here of about $T_{\rm ex} \sim 1600$ K. We conclude that J shocks (with $\boldsymbol{B} \sim 0$) are responsible for the H_2 excitation. *This implies that magnetic fields may not be important in shaping the H_2 disk/envelope.*

In Sect. 4.1 we showed that the estimated visual extinction produces a difference of $A_v \sim 5.4$ mag between the STAR and DISK region. Applying a conversion factor of $N_H = A_v \times 2 \times 10^{21}$ cm^{-2} and assuming that the projected radius of the H_2 feature (5″ = 33 000 AU) induces the difference of 5.4 mag in A_v, we can compute a density contrast between the star and the edge of the disk. The density contrast implies a log (ρ) = 19 (ρ = number density) which is typically expected just after the formation of the initial stellar core in a spherical protostar (see Fig. 2 of Larson 1969). The dimensions at which this density contrast can be expected (~10^{17} cm = 10 000 AU) are consistent with the observed size of the H_2 feature.

We now evaluate the approximate disk/envelope mass, a mass accretion rate and their implications. Based on the narrow-band image and the HK spectrum analysis, we assume an average value of H_2 v = 1–0 S(1) line flux ($F_{S(1)} = 4.39 \times 10^{-17} \pm 5.7 \times 10^{-19}$ W m^{-2} arcsec^{-2}) spread over a disk of angular area ~26 arcsec^2. Using the relation $L_{\rm H_2} = 10 \times F_{S(1)} \times 4\pi {\rm d}^2$ (Davis & Eislöeffel 1995) we obtain $L_{\rm H_2} = 14.5 \pm 0.5\, L_\odot$, where we have assumed a distance of 6.4 kpc. The estimated extinction ($A_v \sim 10$ mag) yields a corrected H_2 luminosity of $L_{\rm H2corr} = L_{\rm H_2} \times 10^{\frac{A_{2.2}}{2.5}} \sim 38.9 \pm 3.8\, L_\odot$.

It is possible to calculate an approximate mass flow rate and a related net H_2 mass using this luminosity. Such a calculation critically depends upon the assumed velocity of the H_2 gas within the disk. If we use an average velocity of 30 km s^{-1}, $L_{\rm H_2} = 38.9 \pm 3.8\, L_\odot$, we obtain a mass accretion rate $\dot{M} = 2L\epsilon/v^2 = 2.6 \pm 0.9 \times 10^{-2}\, M_\odot\, {\rm yr}^{-1}$ for which we used a value of $\epsilon = 50$ (Smith 1995). This accretion rate is about 25 times larger than that for IRAS 20126+4104 where $\dot{M} \sim 1 \times 10^{-3}\, M_\odot\, {\rm yr}^{-1}$ (Cesaroni et al. 1999). This result may not be surprising given that the FIR luminosity of this source is about 5 times higher than that of IRAS 20126+4104. The disk lifetime $R/v = 5360 \pm 1200$ yr combined with the mass accretion rate yields a disk mass of $M_{\rm disk} = 140 \pm 50\, M_\odot$ suggesting that nearly one quarter of the total mass (protostellar envelope = 625 $M_\odot$) is in the form of disk material.

5.3. A massive star, outflow and disk

The results and analysis presented above show a self-consistent picture of a massive YSO associated with an UCHII region, a massive outflow and a massive rotating disk/envelope. IRAS 07427–2400 is a more massive and evolved object than the well-known massive protostar IRAS 20126+4104 (Cesaroni et al. 1999). The luminosity of the star derived from the grey-body model fits indicates an O9-O8.5 type ZAMS star (Panagia 1973) . Despite the ambiguities discussed in Sect. 3.2 the CO J = 1–0 and CO J = 3–2 emission could be tracing a single massive bipolar outflow. Higher spatial resolution observations will be necessary to sort the issue of multiple flows if any. *The observations presented here demonstrate for the first time, a massive rotating disk/envelope visible in H_2 emission.*

The estimated mass accretion rate and disk lifetime strongly support the scenario of massive star formation by

accretion. The interesting question in this case is the future of the mass in the disk/envelope. The estimated disk mass of $M_{\rm disk} \sim 140\ M_\odot$ means that there is sufficient material to form several tens to a hundred low mass stars. Further, the disk is hot at 1600 K and possibly clumpy in nature. The range of velocities from 2 $\rm km\,s^{-1}$ to 40−60 $\rm km\,s^{-1}$ within the disk feature could be explained by assuming a clumpy disk. However, the question is whether this disk/envelope will undergo fragmentation to form several stars or if the material will continue to feed onto the central massive star. We compute the Jeans Mass (p. 303, Lang 1999) using the estimated temperature (1600 K) and an average mass density $\rho \sim 1.4 \times 10^{-19}$ $\rm gm\,cm^{-3}$ based on the 350 μm observations and H_2 observations. The result is $M_J = 2420\ M_\odot >> M_{\rm disk}$. This implies that a warm disk/envelope such as this cannot undergo fragmentation due to insufficient mass.

Given the presence of an UCHII region, it is tempting to think that the central massive star has formed a stable hydrostatic core. The central UCHII region is expected to expand and has the potential to evaporate the disk material. The expansion rate of the UCHII region G5.89–0.39 was measured to be 35 $\rm km\,s^{-1}$ by Acord et al. (1998). If we assume this expansion rate, ∼5000 yrs (∼disk life time) is required for the present epoch UCHII region to expand to the size of the H_2 disk. Alternatively if we just assume a 10 $\rm km\,s^{-1}$ ionized gas sound speed for the expansion velocity, the expansion time will be 16 000 yr (∼3 × disk life time). In any event it is most likely that the UCHII region will expand and evaporate the disk instead of the disk fragmenting or feeding the central star. *In view of these results, the ring structures visible in H_2 emission around massive YSOs (KBD02, De Buizer 2003) may indicate remnants of such an evaporated disk, or cases where a small portion of the envelope is yet to be evaporated.* While the radii of the H_2 emitting features seem too large for a proper accretion disk, a gravitationally bound, flattened structure of this nature is not improbable in view of the observations and arguments presented above. Indeed, even in the case of low mass stars, huge (2000−3000 AU) envelopes that appear as flattened structures are known to exist (Kumar et al. 1999; Weintraub et al. 1994).

6. Summary and conclusions

We present multiwavelength line and continuum observations around a putative disk structure visible in the shock excited H_2 line emission at 2.122 μm.

1) The observations presented here support a scenario for the presence of a massive rotating disk/envelope around the luminous YSO IRAS 07427–2400 associated with an UCHII region. Its association with a massive bipolar outflow and a massive disk/envelope makes this one of the most massive YSOs known to date forming via accretion. The disk-like feature seen in H_2 emission is found to be perpendicular to the outflow axis and strongly coincides with dense gas tracers indicative of circumstellar disks/envelopes. *PV* diagram of the $C^{18}O$ map indicates a rotating core with a velocity gradient of ~ 0.1 $\rm km\,s^{-1}$ $\rm arcsec^{-1}$.

2) Near-infrared *H* & *K*–band spectra of the H_2 feature show several ro-vibrational emission lines of H_2, the ratios of which indicate shock excitation of H_2. We measure an excitation temperature of ∼1600 K, and an average extinction of $A_v = 11$ mag in the line emitting regions. Further, the measured H_2 fluxes and detection of [FeII] lines indicate the presence of J shocks rather than C shocks. The detection of Br γ emission close to the central source can be explained with fast J shocks alone, although contributions from the UCHII region cannot be ruled out.

3) Using the measured line fluxes, we estimate an envelope mass accretion rate $\dot{M} \sim 2.6 \pm 0.9 \times 10^{-2}\ M_\odot\,\rm yr^{-1}$ and a life time of ∼5400 yr resulting in a mass of 140 ± 50 $M_\odot$. Computation of the Jeans Mass for the observed disk/envelope temperature and number densities indicate that the disk/envelope can not undergo fragmentation. High spatial and spectral resolution observations at near-infrared wavelengths can throw much light onto the detailed properties of the disk/envelope structure and the source of excitation of the H_2 emission.

Acknowledgements. The United Kingdom Infrared Telescope is operated by the Joint Astronomy Center on behalf of the UK Particle Physics and Astronomy Research Council. The UKIRT data reported here were obtained as part of its Service Pro gramme. Observations at the CSO are supported by NSF grant AST-9980846. This research made use of data products from the Midcourse Space Experiment. Processing of the data was funded by the Ballistic Missile Defence Organization with additional support from NASA office of Space Science. This Research has also made use of the NASA/IPAC Infrared Science Archive, which is operated by the Jet Propulsion Laboratory, California Institute of Technology, under contract with the National Aeronautics and Space Administration. We thank an anonymous referee for many useful suggestions.

References

Acord, J. M., Churchwell, E., & Wood, D. O. S. 1998, ApJ, 495, L107
Bachiller, R. 1996, ARA&A, 34, 111
Bally, J., O'Dell, C. R., & McCaughrean, M. J. 2000, AJ, 119, 2919
Beckwith, S. 1999, in The Origin of Stars and Planetary Systems, ed. C. J. Lada, & N. Kylafis, NATO Science Series (The Netherlands: Kluwer Publishers)
Beckwith, S. V. W., Henning, T., & Nakagawa, Y. 2000, in Protostars & Planets IV, ed. V. Mannings, A. P. Boss, & S. S. Russell (University of Arizona Space Science Series)
Beckwith, S., & Sargent, A. I. 1991, ApJ, 381, 250
Beckwith, S., & Sargent, A. I. 1996, Nature, 383, 139
Black, J., & van Dishoeck, E. 1987, ApJ, 322, 412
Le Bourlot, J., Pineau des Forêts, G., Flower, D. R., & Cabrit, S. 2002, MNRAS, 332, 985
Brand, P., Moorhouse, A., Burton, M., et al. 1988, ApJ, 334, L103
Burton, M., Geballe, T., & Brand, P. 1989, MNRAS, 238, 1513
De Buizer, J. M. 2003, MNRAS, 341, 277
Cesaroni, R., Felli, M., Jenness, T., et al. 1999, A&A, 345, 949
Dutrey, A., Guilloteau, S., Duvert, G., et al. 1996, A&A, 309, 493
Davis, C. J., & Eislöeffel, J. 1995, A&A, 300, 851
Fernandes, A. J. L., Brand, P. W. J., & Burton, M. G. 1997, MNRAS, 290, 216
Draine, B. 1989, Proc. 22nd Eslab Symp., Infrared Spectroscopy in Astronomy (ESA Publications Ltd, Salamanca), 93
Fridlund, C. V. M., Sandqvist, A., Nordh, H. L., & Olofsson, G. 1989, A&A, 213, 310

Gezari, D. Y., Schmitz, M., Pitts, P. S., & Mead, J. M. 1993, Catalog of Infrared Observations, 3rd ed. (NASA Reference Publications), 1294
Gredel, R. 1994, A&A, 292, 580
Henning, T., Cesaroni, R., Walmsley, M., & Pfau, W. 1992, A&AS, 93, 525
Herbst, T. M., Koresko, C. D., & Leinert, Ch. 1995, ApJ, 444, 93
Hildebrand, R. H. 1983, QJRAS, 24, 267
Hogerheijde, M. R., & Sandell, G. 2000, ApJ, 534, 880
Hollenbach, D. J., & McKee, C. F. 1989, ApJ, 342, 306
Hughes, V. A., & MacLeod, G. C. 1993, AJ, 105, 1495
Koresko, C. D., Herbst, T. M., & Leinert, Ch. 1997, ApJ, 480, 741
Kumar, M. S. N., Anandarao, B. G., & Davis, C. J. 1999, A&A, 344, L9
Kumar, M. S. N., Bachiller, R., & Davis, C. J. 2002, ApJ, 576, 313 (KBD02)
Lang, K. R. 1999, Astrophysical Formulae, 3rd ed., vol. 1 (A&A Library Series, Springer Verlag Publications)
Larson, R. B. 1969, MNRAS, 145, 271
MacLeod, G. C. 1991, MNRAS, 252, 36
Muench, A. A., João, A., Lada, C. J., & Lada, E. A. 2001, ApJ, 558, L51
Nisini, B., Caratti o Garatti, A., Giannini, T., & Lorenzetti, D. 2002, A&A, 393, 1035
Padgett, D. L., Brandner, W., Stapelfeldt, K. R., et al. 1999, AJ, 117, 1490
Panagia, N. 1973, AJ, 78, 929
Seal, P., & Shivanandan, K. 1989, Bull. Astro. Soc. India, 17, 27
Shepherd, D., & Churchwell, E. 1996, ApJ, 457, 267 (SC96)
Shepherd, D., & Kurtz, S. E. 1999, ApJ, 523, 690
Shepherd, D., Claussen, M. J., & Kurtz, S. 2001, Science, 292, 1513
Shu, F. H., Najita, J. R., Shang, H., & Li, Z.-Y. 2000, in Protostars and Planets IV, ed. V. Mannings, A. P. Boss, & S. S. Russell (Tucson: Univ. Arizona Press), 789
Smits, D. P. 1994, MNRAS, 269, L11
Smith, M. D. 1993, ApJ, 406, 520
Smith, M. D. 1994, MNRAS, 266, 238
Smith, M. D. 1995, A&A, 296, 789
Slysh, V. T., Dzura, A. M., Val'tts, I. E., & Gerard, E. 1997, A&AS, 124, 525
Weintraub, D. A., Tegler, S. C., Kastner, J. H., & Rettig, T. 1994, ApJ, 423, 674
Zhang, Q., Hunter, T. R., Sridharan, T. K., & Ho, P. T. P. 2002, ApJ, 566, 982